THE ASTROPHYSICAL JOURNAL, 323:433–450, 1987 December 15

THE STELLAR POPULATIONS OF SHAPLEY CONSTELLATION III[1]

NEILL REID
Royal Greenwich Observatory and California Institute of Technology

JEREMY MOULD
California Institute of Technology

AND

IAN THOMPSON
Mount Wilson and Las Campanas Observatories
Received 1987 March 26; accepted 1987 May 19

ABSTRACT

We have constructed a $V-I$ color-magnitude diagram for a 0.6 deg^2 field covering part of the star formation region Shapley III in the LMC. The main-sequence stars have a luminosity function exhibiting a pronounced break at $M_v \sim -3$ which we identify with the turnoff of the first star-forming burst. Using this as an age indicator, we have compared stellar evolutionary models with the dynamical age estimate determined by Dopita, Mathewson, and Ford and derive the initial luminosity and mass functions. Although the star formation history in the region is more complex than the DMF model, the "dynamical clock" in Shapley III is in better agreement with the "stellar evolutionary clock" if models with little or no convective overshoot are adopted. Our results are sensitive to the star forming rate adopted. Finally, the luminosity function of the intermediate-age population red giants yields a distance modulus for the LMC of 18.4 ± 0.15.

Subject headings: galaxies: distances — galaxies: Magellanic Clouds — stars: evolution — stars: stellar statistics

I. INTRODUCTION

A cursory study of modern photographic plates of the Large Magellanic Cloud shows that the brighter stars cluster in various regions around the Bar. This clumping was originally noticed by Nail and Shapley (1953), who identified a number of "constellations" and first suggested that these might constitute bursts of star formation. Since then, studies of more distant galaxies have shown that such bursts of activity are common in irregular galaxies (Gallagher, Hunter, and Tutukov 1984). These observations have cosmological implications, since it is by no means clear how such relatively low mass systems have retained sufficient gas to indulge in such spectacular outbursts. Clearly the proximity of the Magellanic Clouds make them the optimum laboratories for studying the characteristics of starburst regions.

Shapley Constellation III is one of the largest regions of star formation in the Large Cloud. The UKST Hα survey by Goudis and Meaburn (1978) and Meaburn (1980) reveals an obvious ring of H II regions, centered on R.A. $\sim 5^h31^m$, decl. $\sim -66°55'$, while young star clusters are distributed throughout the area (Lucke and Hodge 1970). These features are also clear in the *IRAS* maps of emission from hot dust. The McGee and Milton (1966*a*, *b*) 21 cm survey shows a surrounding shell of neutral hydrogen, and Dopita, Mathewson, and Ford (1985; hereinafter DMF) have recently conducted a detailed H I survey using the Parkes 64 m dish. Using these data, together with observations of the brightest stars in the Lucke and Hodge clusters, DMF have suggested that Shapley III is a region of self-propagating star formation with the initial, triggering burst 15 Myr ago and subsequent shell-like expansion. We shall return to this model in more detail in § III.

Previous studies, then, have concentrated on the gaseous component of Shapley III and on the star clusters. In this paper we present the first extensive study of the field stars within Shapley III and use their distribution, both spatially and in the color-magnitude diagram, to constrain the star-formation history. In the following sections we first give details of the observational data and the construction of the color-magnitude diagram. We show that there have been at least two distinct episodes of star formation, with the young stars from the recent starburst overlying a more extensive older population of red giant branch stars. In § III we discuss the characteristics of the young stars, while the older population is dealt with in § IV. Section V presents our conclusions.

II. OBSERVATIONS, DATA REDUCTION, AND THE COLOR-MAGNITUDE DIAGRAM

Our photometry is based on four V and two I band plates taken on the du Pont 2.5 m at Las Campanas (Table 1). The V plates were hypered by baking in forming gas, while the IV-N were wet-hypered using silver nitrate solution. These plates were scanned and digitized on the COSMOS facility at the Royal Observatory, Edinburgh. Our reduction methods are discussed at length in Reid and Mould (1984; hereinafter Paper I), and we will not repeat these details here. The UKST plates analyzed in Paper I cover Shapley III, but the high star density and consequent overlapping of images led to our excluding the region from our initial survey. The sixfold increase in scale obtained from using the du Pont plates largely circumvents these problems. We are still unable to achieve accurate photometry of stars within H II regions, which introduces a slight bias against our identifying stars in the youngest clusters.

[1] Based on observations obtained at the Las Campanas Observatory of the Carnegie Institution of Washington as part of the agreement between the California Institute of Technology and the Carnegie Institute of Washington.

TABLE 1

PLATE LOG

Plate	Emulsion	Filter	Exposure (minutes)	Epoch (1984)
CD 2578..........	IIa-D	GG 495?	45	Oct 31
CD 2579..........	IIa-D	GG 495?	45	Oct 31
CD 2580..........	IIa-D	GG 495?	20	Oct 31
CD 2588..........	IIa-D	GG 495?	45	Nov 1
CD 2586..........	IV-N	Wr 89B	60	Nov 1
CD 2587..........	IV-N	Wr 89B	60	Nov 1

However, the areas affected comprise only a few percent of the total area covered.

The plates are centered at R.A. = $5^h31^m58^s$, decl. = $-67°12'.2$ (1950) and extend over a field of $\sim 45' \times 45'$ (0.6 deg^2). We therefore cover the lower half of Meaburn's supergiant shell LMC 4 (Meaburn 1980), including the OB association LH 77, or Shapley III (Lucke and Hodge 1970). Other LH associations in the field are LH 65, 70, 79, 84, 86, and 92.

The COSMOS scans of the photographic plates were photometrically calibrated from standard star sequences set up using V and I CCD frames obtained at Cerro Tololo Inter-American Observatory and at Las Campanas. The former observations were made on the 4 m using the prime-focus camera and consist of two fields near NGC 2004 and one near NGC 2034. In addition, we obtained V and I exposures in four other fields, giving full coverage of the 1 deg^2 field. We used the 1 m Swope telescope for the latter observations. The CCD observations were reduced using standard techniques (see Mould, Kristian, and DaCosta 1983) and the final sequences placed on the Johnson V and Cousins I systems.

In reducing the photographic data, we first transformed the measurements onto a single instrumental "magnitude" scale in each passband. We used plate CD 2579 as the standard V plate and CD 2586 in I. Since all stars in common between the two plates are used, these transformations are better defined than the "standard" calibrations for individual plates. The resultant instrumental system is then tied to the standard system using the mean "magnitudes" for each of the photometric standards. As Figure 1 shows, the photographic I band system (IV-N + Wr 89B filter) is well matched to the Cousins system. The rms scatter about the mean curve is only 0.14 mag. However, the V calibration proved (surprisingly) more awkward. Although we were nominally using the standard V combination of GG 495 filter + IIa-D emulsion, a large color term was evident in the data. We defined the instrumental magnitude, v, using our bluest calibrators, with $V-I < 0.2$. Figure 2 plots the residuals V-v against v-I. There is clearly a strong color term present, such that blue stars have brighter instrumental magnitudes than red stars with equal V magnitudes. Applying the mean relation from Figure 2, however, adequately corrects for this blue leak, as the final V calibration curve (Fig. 3) shows. The rms scatter is $\sigma = 0.17$ mag.

Our final photometric accuracy we estimate as ~ 0.08 mag in I (for stars with good images two I plates and with $I < 17$) and ~ 0.05 in V (for stars on four V plates and with $V < 18$). We further define "good" images below. These uncertainties are derived from the plate-to-plate residuals and therefore accurately reflect the internal magnitude errors. The large V color term almost certainly leads to systematic residuals with respect to the standard systems. However, we do not expect such systematic errors to exceed 0.1 mag in the range $0 < V-I < 2.0$. When we come to discuss the width of features in the H-R diagram, we expect that the internal errors noted above are appropriate.

We have already mentioned that the large plate-scale of $10''.9$ mm^{-1} at the $f/7.5$ Cassegrain focus of the du Pont 2.5 m allows us to examine regions with high star density. However, a certain degree of merging is still present. As in Paper I, we have

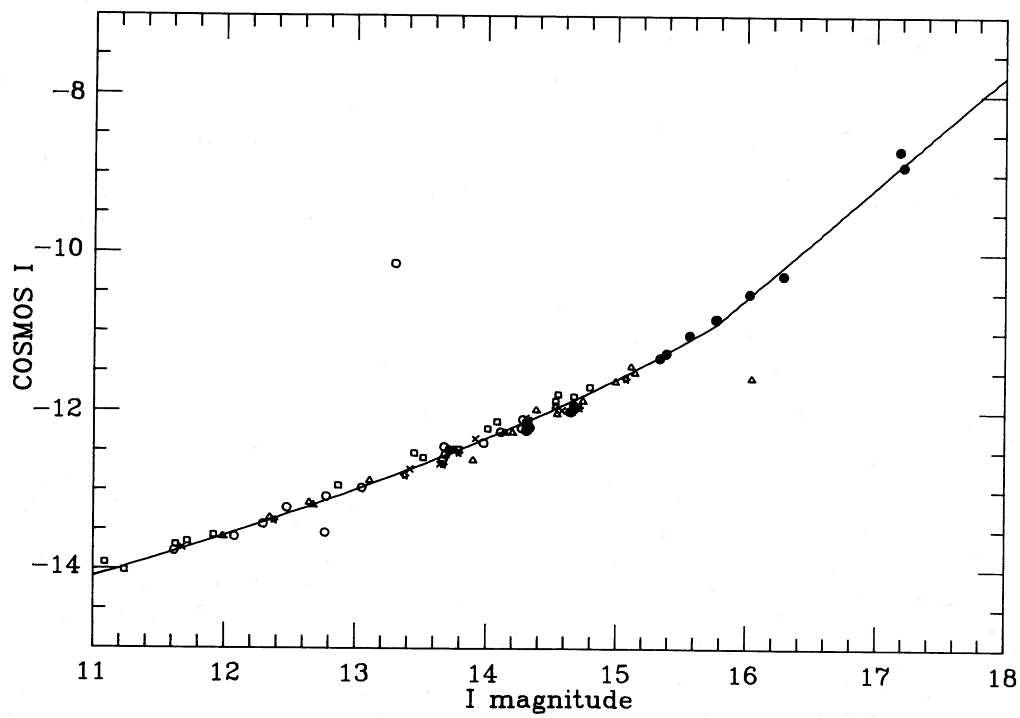

FIG. 1.—Calibration curve for the I band photographic data

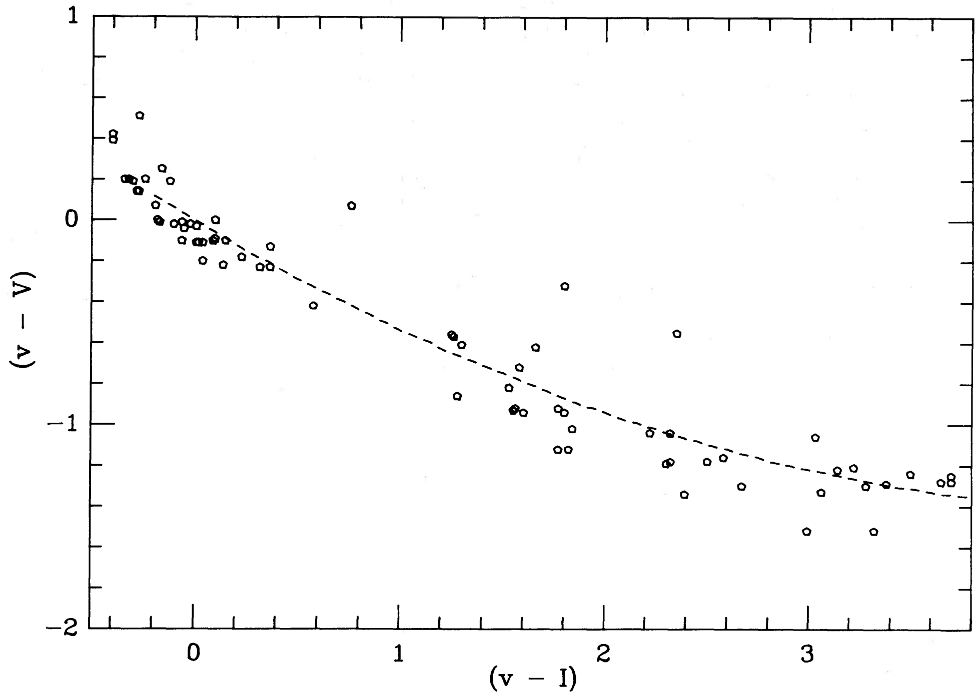

FIG. 2.—Color term in the V band data; v is the instrumental calibration defined by the bluer standards, as described in the text

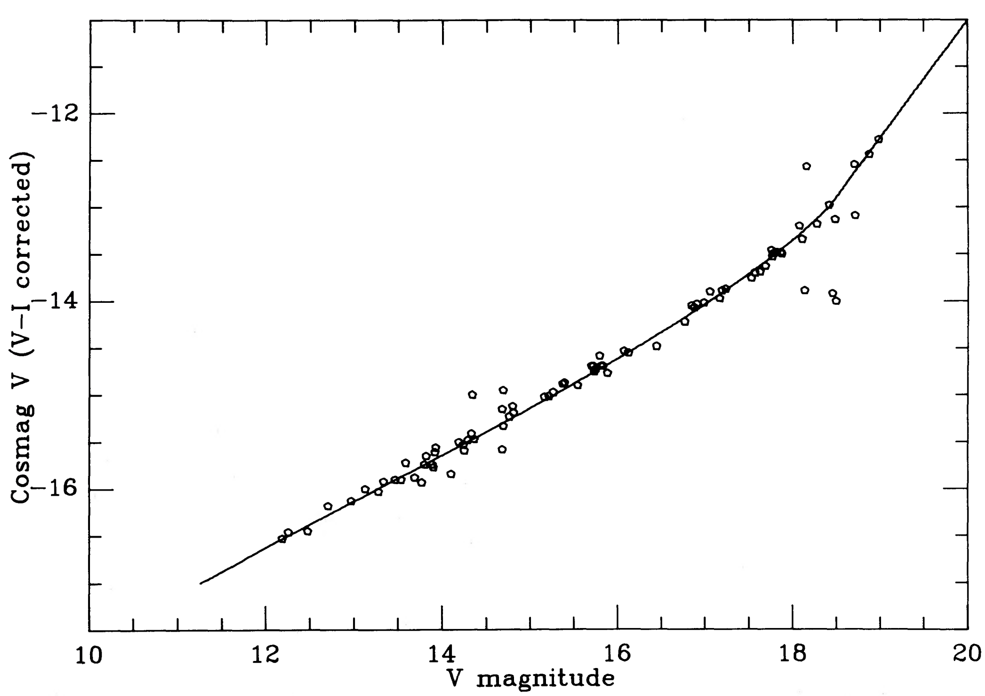

FIG. 3.—Final V calibration curve, allowing for the color term

used the COSMOS image-shape parameters to exclude automatically these merged images. Inspection of the plates shows that an eccentricity of $\epsilon \sim 0.70$ is an appropriate limit for the I plates, while the images are photometrically acceptable to $\epsilon \sim 0.65$ on the II-ad plates. We have defined our final sample as including all stars with at least one acceptable measure in I and one V image with $\epsilon_V > 0.65$, with the further criterion that the star is detected on at least three V plates.

We have assessed the completeness of our sample in several ways. First, we determined the proportion of images with "good" photometry relative to all images as a function of magnitude in both V and I. While the magnitudes measured for the more elongated objects (two, three star mergers) are less accurate, this procedure does give a general guide to systematic trends. Figure 4*a* shows that incompleteness, judged in this manner, is relatively constant at $\sim$7% to $I \sim 17$ and 20%–30% in V to $V \sim 18$. However, we require good photometry in both passbands for a color-magnitude diagram. Figure 4*b* shows the fraction of stars with good photometry in both V and I as a function of apparent magnitude in V (the "V

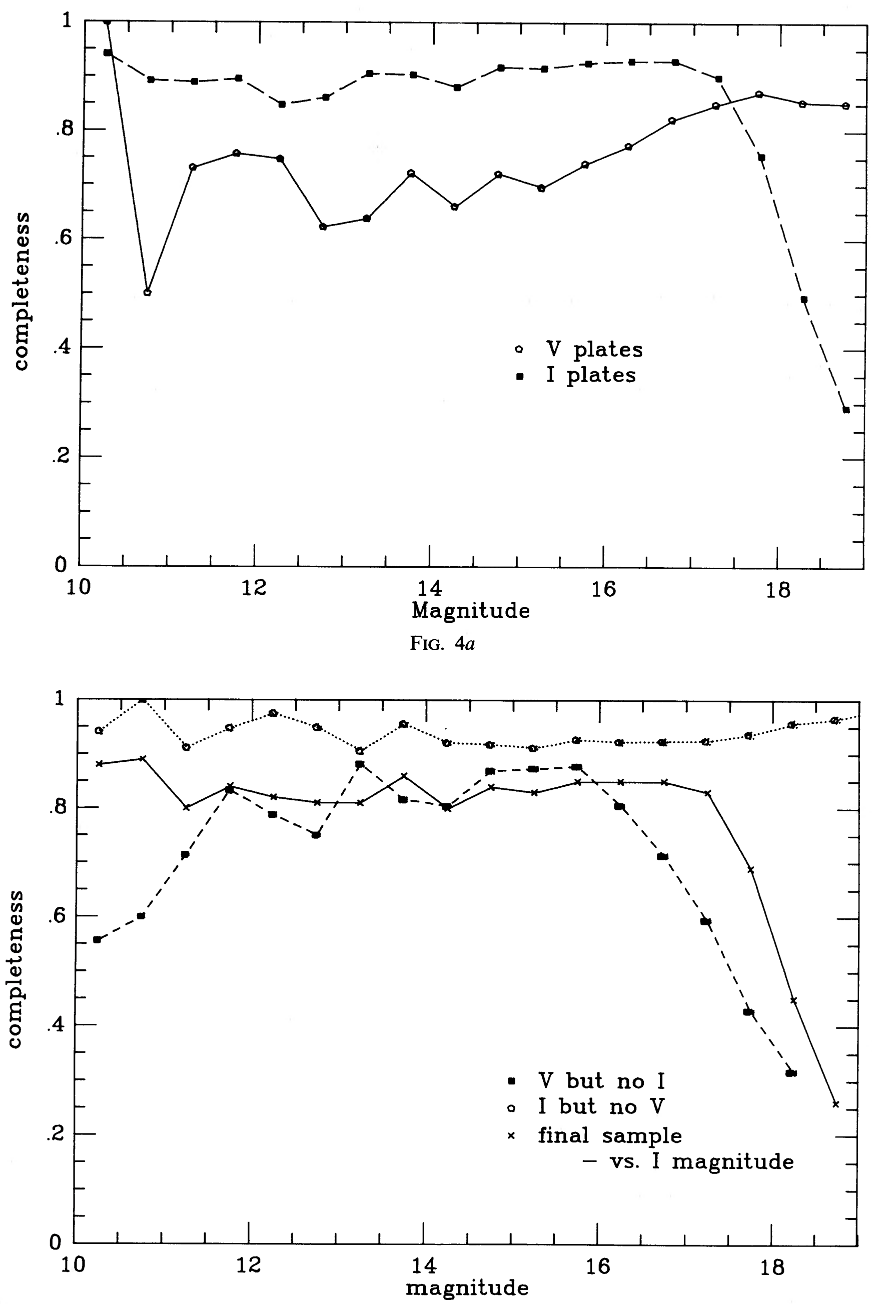

FIG. 4*a*

FIG. 4*b*

FIG. 4.—Incompleteness in our survey. (*a*) Percentage of objects with good images (as defined in the text) as a function of magnitude on the V and I plates, respectively. (*b*) Fraction of stars with good images on both V and I photographic COSMOS scans. The completeness curves are plotted as a function of I magnitude (labeled "I but no V") and V magnitude ("V but no I"). The fractional completeness (as a function of I magnitude) adopted for the final sample is also shown.

but no I" curve) and in I (the "I but no V" curve). Note that there are ~ 3 times as many stars with $I < 17$ as with $V < 17$. The decline in completeness in the "V but no I" curve is partly due to the larger absolute number of contaminated images on the I plate.

In this paper we are particularly aiming at determining the true variation of number densities of stars with magnitude in the LMC. Hence we are concerned with avoiding differential incompleteness. Figure 4*b* shows our estimate of the absolute completeness of our data as a function of I magnitude. This function is approximately constant to $I \sim 16$, but declines toward fainter magnitudes. To allow for this we have applied corrections of from 5% to 20% to our main-sequence star counts from $\langle I \rangle$ of 16 to 17. These corrections are shown in column four for Table 4. This adjusts all our data to approximately the same level of incompleteness, which, allowing for double stars, we estimate as $\sim 60\%$ (i.e., 40% excluded from our final sample).

Table 2 presents the stellar number counts with magnitude and color and the color-magnitude diagram is shown in Figure 5. Neither is corrected for incompleteness at any level, nor are the data dereddened. These clearly show two well-defined features—a blue main-sequence due to young, recently formed massive stars and a well-developed, extended red giant branch. Less obvious, but nonetheless present at $I \sim 11$–12, is a small clump of red supergiants also associated with the younger population.

Apart form the two LMC populations, Figure 5 also includes a contribution from foreground galactic stars. We have used a modified version of Gilmore's (1984) star count model to assess the extent of the contamination and the resulting color-magnitude distribution for this field is given in Table 3. The model includes three components—a thin exponential disk, including both old disk ($M_v > +4$, z_0 exponential scale height of 300 pc) and young disk (z_0 of 100 pc); an intermediate component ("thick disk") with an evolved (47 Tucanae like) luminosity function, $z_0 \sim 1300$ pc, and a local density of 1.5% of the thin disk; and the halo, with a de Vau-

TABLE 2

STELLAR NUMBER COUNTS

I	V−I																		
MAGNITUDE	−0.90	−0.70	−0.50	−0.30	−0.10	0.10	0.30	0.50	0.70	0.90	1.10	1.30	1.50	1.70	1.90	2.10	2.30	2.50	2.70
9.13..........					1				1			1							
9.38..........				1					1							1			1
9.63..........									1				1			1			1
9.88..........								1	1		1								
10.13..........								1		1									1
10.28..........									1	1		2		1	1				
10.63..........							2	1	1	1	3		2	1		1	1	1	
10.88..........						1				1	1	3	1	2	1	1	1	3	
11.13..........									1	2	1	2					6	2	
11.38..........						1	3	2	1		1	2			1	1	3	1	1
11.63..........					1	2		3	2	2	1	2	1	2	8	7	2	1	
11.88..........		1			1	3	2	5	1	1	2	1	1	4	11	3			1
12.13..........		2			4	2	3	3	1	3	3	3		2	5	3			
12.38..........				1	7	4	1	1	3	6	1	1	2	2	2	1	1	1	
12.63..........					4	5	2	1	1	4	1			2	2	1			
12.88..........			1	1	6	7	2	1	3	4	2	2	2	3	1	1			
13.13..........	1	1		4	8	8	3	1	3	8	1	1	1	1	2			1	1
13.38..........			1	5	9	9	3	1	9	3	5	2	2	3	1	1	1	3	2
13.63..........	1			3	16	10	4	2	9	9	6	1	5	7			1	3	3
13.88..........		1	2	7	26	8	3	2	12	13	2	6	6	2	3	5	9	9	3
14.13..........		1	6	7	19	19	3	8	3	13	7	5	6	5	1	11	6	6	5
14.38..........		1	1	13	38	21	3	1	10	17	9	5	10	10	15	11	6		1
14.63..........	1	3	2	14	59	20	3	9	17	12	9	16	12	22	36	22	2		2
14.88..........	1	4	3	28	55	20	1	6	12	11	14	12	15	40	51	9	2		1
15.13..........		4	7	30	61	21	2	8	17	19	12	27	33	50	18	5	3	3	1
15.33..........	2	8	4	36	88	15	9	12	19	17	21	22	72	42	15	5	3	1	2
15.63..........	4	4	9	60	92	16	5	11	27	17	38	54	74	18	2	2	1		
15.88..........	3	6	19	94	164	14	13	20	35	40	53	115	85	12	2	1	1	1	1
16.13..........	6	9	15	100	185	18	11	19	46	58	76	179	52	5	2	2	1	1	1
16.38..........	4	12	19	112	227	13	20	18	43	79	176	179	24	4	7	3	1		
16.63..........	9	16	23	139	239	25	15	26	57	104	275	100	9	6	3	1			
16.88..........	10	12	34	161	261	34	20	24	83	191	299	55	8	4	3	1	1		
17.13..........	9	19	29	193	273	37	32	34	178	317	193	29	9	3	2				
17.38..........	30	12	31	239	252	37	21	90	232	255	84	18	3	3	1				
17.63..........	70	20	35	259	228	51	63	110	258	192	47	11	4		1				
17.88..........	67	15	24	269	186	46	60	105	227	107	30	1	1		1				
18.13..........	35	9	18	133	86	32	29	85	160	60	14	2	2						
18.38..........	19	14	19	94	44	14	34	78	96	28	1	1							
18.63..........	11	11	26	64	27	12	37	73	50	6	4	1							
18.88..........	4	4	22	48	18	11	37	43	12	2									
19.13..........	3	3	39	26	5	9	33	13	2	1									
19.38..........	1	7	25	17	9	13	11	3											
19.63..........	2	13	28	13	10	17	2												
19.88..........		1	6	1	2	2													

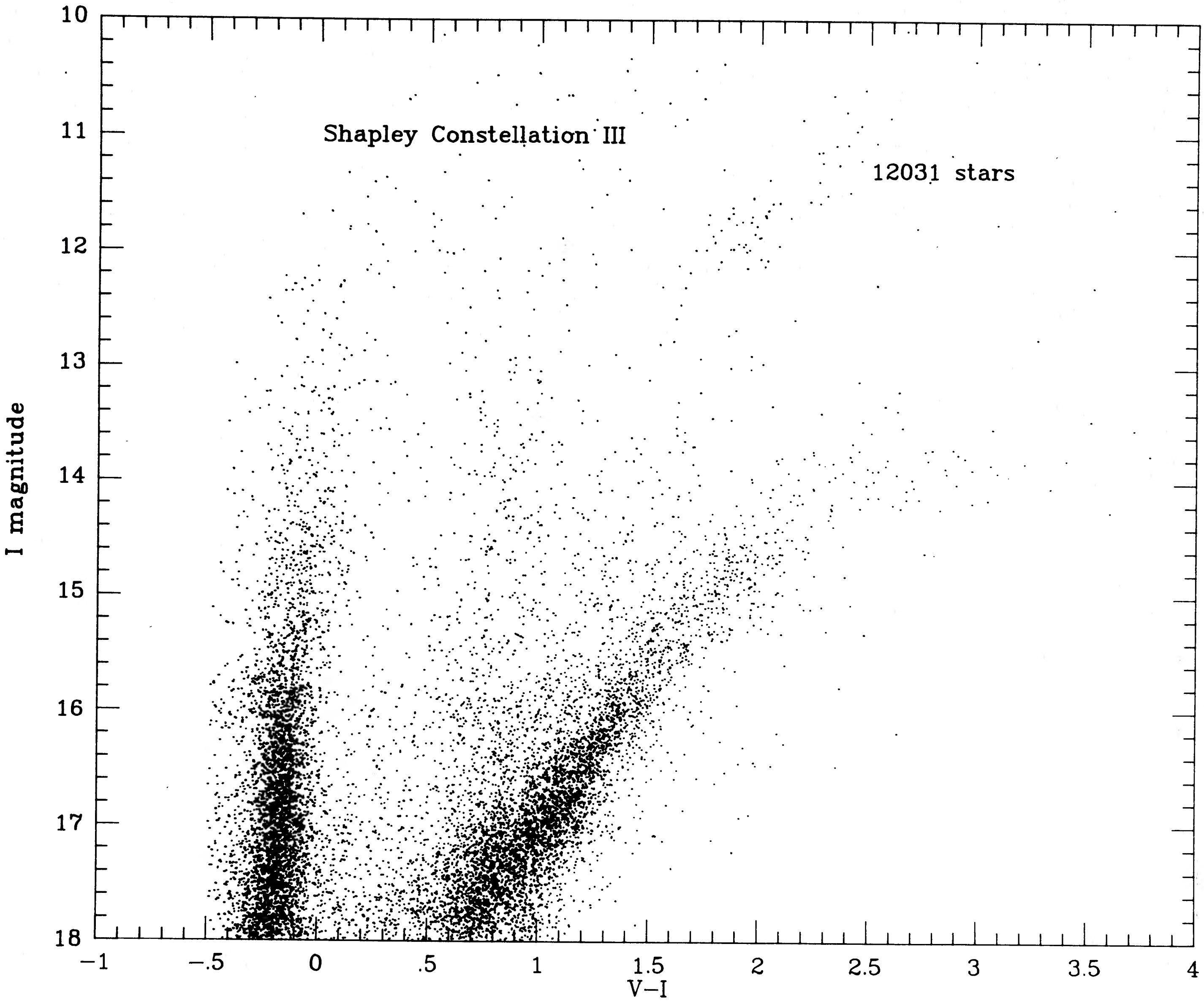

FIG. 5.—Color-magnitude diagram for Shapley III

couleurs spheriod density distribution, axial ratio 0.9, and local density 0.15% of the disk. The disk population dominates the star counts, with the overall ratios 0.77 : 0.14 : 0.09 (in the sense disk : intermediate : halo) for $I < 17$. As is now well known, the old disk contributes the red stars in Table 3, while the G stars are subgiants and main-sequence subdwarfs from the intermediate and extended halo populations. Neither contribute significant numbers—the halo stars fall between the main sequence and the red giant branch.

In the following sections we discuss first the characteristics of the young main-sequence stars before moving on to consider the old giant branch population.

III. THE MAIN-SEQUENCE POPULATION

a) The Luminosity Function

There is a clear division between the main sequence and giant branch stars in Figure 5. We have used this fact to construct a luminosity function for the former population, including all stars with $V-I < 0.0$. As Table 4 indicates, foreground contamination is negligible and we have not applied any corrections. Before deriving absolute magnitudes we must allow for interstellar absorption, both within our Galaxy and in the LMC. McNamara and Feltz (1980) have determined the foreground absorption as $E_{B-V} \sim 0.034$, or $A_v = 0.1$ mag, for the area of Shapley III. We can use the DMF H I survey to estimate the absorption due to LMC material. Obviously the neutral gas is distributed in a distinctly nonuniform way, being substantially more dense where star formation is still going on. Dopita, Mathewson, and Ford's (1985) observations show that H I reaches densities of $\sim 24 \times 10^{20}$ atoms cm^{-2} in these areas ($E_{B-V} \sim 0.12$), while the density falls to less than 10^{20} cm^{-2} in the center of the ring. Our photographic data are almost entirely in the lower density regime, with E_{B-V}(LMC) $< \sim 0.04$, since the gaseous emission near the H I clumps rules out stellar photometry in these regions. Hence we have assumed a mean A_v of 0.2 mag.

Finally, we adopt a distance modulus to the LMC of 18.35

TABLE 3

FOREGROUND STARS PER SQUARE DEGREE

		$V-I$											
I	POPULATION	−0.1	0.1	0.3	0.5	0.7	0.9	1.1	1.3	1.5	1.7	1.9	2.1
10.5..........	Disk	...	0.1	0.7	7.1	5.1	3.9	3.4	1.3	0.2	...	...	0.1
	IP	...	...	...	...	0.7	2.6	0.8	0.2	0.1	0.1	...	...
	Halo	...	...	0.1	0.2	...	...	...	...	...	...	...	...
	Total	...	0.1	0.7	7.2	5.3	4.6	6.0	2.1	0.4	0.1	0.1	0.1
11.5..........	Disk	...	...	0.4	13.8	14.7	7.3	5.0	1.8	0.5	0.3	0.2	0.3
	IP	...	...	...	0.2	0.3	2.0	4.9	1.1	0.2	0.1	...	...
	Halo	...	0.3	...	0.3	0.6	0.2	0.1	...	...	...	...	...
	Total	...	0.3	0.4	14.3	15.6	9.5	10.0	2.9	0.7	0.4	0.2	0.3
12.5..........	Disk	...	...	...	18.6	36.1	12.3	9.4	3.6	1.7	1.1	0.6	1.0
	IP	...	...	...	0.7	1.1	4.1	5.8	0.7	...	...	...	...
	Halo	0.1	1.0	...	1.0	1.9	0.5	0.1	...	...	...	...	...
	Total	0.1	1.0	...	20.3	39.1	16.9	15.6	4.3	1.7	1.1	0.6	1.0
13.5..........	Disk	...	...	...	15.4	69.4	25.1	22.9	10.9	5.3	3.7	4.1	4.5
	IP	...	...	...	2.3	3.4	10.3	3.2	0.1	...	...	...	...
	Halo	0.4	2.6	...	2.5	5.2	11.1	0.2	...	...	...	...	...
	Total	0.4	2.6	...	20.2	78.0	36.5	26.3	11.0	5.3	3.7	4.1	4.5
14.5..........	Disk	...	...	...	6.2	95.7	53.4	49.2	27.6	15.0	11.3	6.7	13.8
	IP	...	...	...	7.2	9.2	14.4	0.9	0.2	...	...	...	...
	Halo	1.3	5.0	...	4.1	11.4	1.6	0.2	...	...	...	...	...
	Total	1.3	5.0	...	18.1	118	69.4	50.3	27.8	15.0	11.3	6.7	13.8
15.5..........	Disk	...	...	...	0.8	82.8	86.7	73.9	53.4	34.1	29.3	19.3	37.5
	IP	...	...	...	20.0	26.9	23.4	1.8	0.6	0.2	0.3	0.1	...
	Halo	2.8	6.2	...	7.7	22.9	7.8	0.2	...	...	...	...	...
	Total	2.8	6.2	...	28.5	132	118	75.9	54.0	34.3	29.6	19.4	37.5
16.5..........	Disk	...	...	...	...	36.3	84.2	63.0	67.9	56.1	58.6	45.5	80.6
	IP	...	...	...	42.8	56.3	17.3	5.8	2.3	0.5	1.0	0.4	0.9
	Halo	4.1	5.1	...	17.2	30.9	1.3	0.2	...	...	...	...	...
	Total	4.1	5.1	...	60.0	124	103	69.0	70.2	56.6	59.6	45.9	81.5
17.5..........	Disk	...	...	...	...	5.5	37.2	22.0	44.1	54.8	78.3	79.4	122
	IP	...	...	...	61.0	115	26.5	17.1	7.2	1.8	3.6	1.3	3.1
	Halo	3.9	3.0	...	45.8	32.7	1.6	0.3	0.1	...	...	...	...
	Total	3.9	3.0	...	107	153	65.3	39.4	51.4	56.6	81.9	86.7	125

(Reid and Strugnell 1986). Thus

$$\langle M_v \rangle = \langle I \rangle - 18.675 .$$

The resultant luminosity function is given in Table 4 and plotted in Figure 6. Column (3) in the table gives the actual number of stars observed, and column (4) gives the incompleteness corrections applied to the faintest bins. These latter factors are included in the logarithmic luminosity function tabulated in column (5). Column (6) gives the stellar mass calibration that we have adopted, and the resulting mass function is shown in the final column of the table. We can represent our results for the luminosity function as three power-law segments of the form

$$\phi(M_v) \propto M_v^{\gamma} ,$$

with

$$\gamma \sim 0.55 , \quad M_v < -4 ,$$

$$\gamma \sim 0.32 , \quad -4 < M_v < -3 ,$$

$$\gamma \sim 0.30 , \quad -3 < M_v .$$

There is a clear break in the luminosity function between $M_v = -3$ and -2.8, corresponding to $\langle I \rangle \sim 15.5$. As discussed in § II, we have no reason to suspect differential incompleteness or other machine-induced effects at this magnitude, and we interpret this as the main-sequence turnoff in LMC 4. Allowing for incompleteness fainter than $M_v = -3$ gives the slope of 0.3 quoted above—without these corrections, the slope derived is much flatter at ~0.22. We return to this point in § III*b*.

Other derivations of the stellar luminosity function over this

TABLE 4

THE LUMINOSITY FUNCTION

$\langle I \rangle$	M_v	N	Percent	log (N)	log (mass)	ψ(log m)
12.625..........	−6.05	5	...	0.699	1.69	...
12.875..........	−5.80	7	...	0.845	1.64	...
13.125..........	−5.55	13	...	1.114	1.59	...
13.375..........	−5.30	15	...	1.176	1.54	1.98
13.625..........	−5.05	20	...	1.301	1.49	2.08
13.875..........	−4.80	36	...	1.556	1.44	2.28
14.125..........	−4.55	35	...	1.544	1.39	2.22
14.375..........	−4.30	52	...	1.716	1.34	2.35
14.625..........	−4.05	78	...	1.892	1.29	2.50
14.875..........	−3.80	91	...	1.959	1.24	2.51
15.125..........	−3.55	102	...	2.009	1.19	2.50
15.375..........	−3.30	139	...	2.143	1.14	2.58
15.625..........	−3.05	162	...	2.210	1.09	2.66
15.875..........	−2.80	282	...	2.450	1.06	2.93
16.125..........	−2.55	308	5	2.509	1.03	2.94
16.375..........	−2.30	370	10	2.610	0.98	2.91
16.625..........	−2.05	410	15	2.674	0.93	2.97
16.875..........	−1.80	468	20	2.749	0.88	3.05

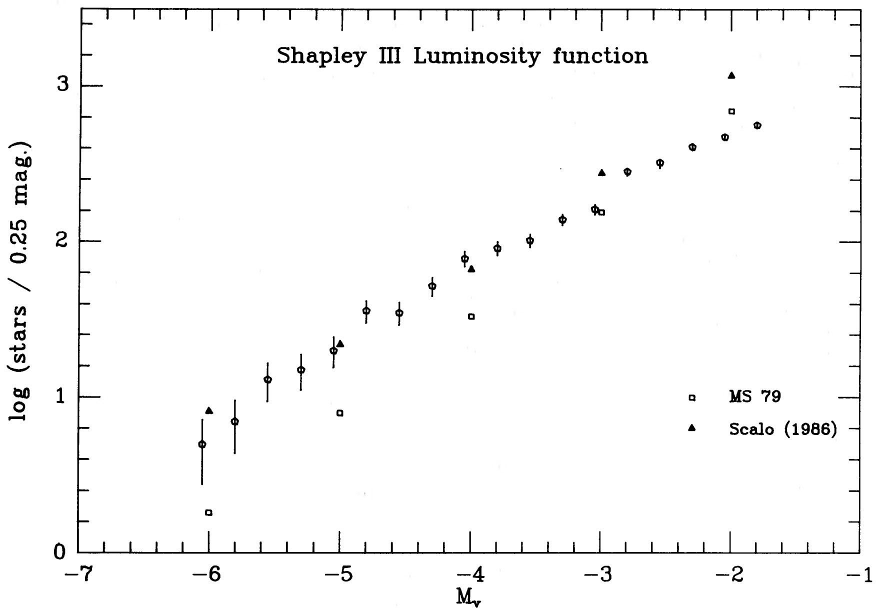

FIG. 6.—Luminosity function defined by the main-sequence stars in Shapley III. The Miller and Scalo (1979) and Scalo (1986) Galactic star luminosity functions appropriately scaled are also shown.

range in M_v are relatively scarce. Miller and Scalo (1979) reviewed a number of such derivations for the stars in the "solar neighborhood," arriving at a luminosity function

$$\phi(M_v) \propto M_v^{0.6} ,$$

This is essentially McCuskey's (1966) luminosity function. Scalo has recently returned to the subject in an extensive review (Scalo 1986). From a combination of Galactic surveys, he has derived a luminosity function which does not fit a single power law, but steepens toward fainter absolute magnitudes (Fig. 6).

Clearly the Galactic luminosity function is much steeper than the LMC data at magnitudes fainter than $M_v \sim -3$. In all probability this simply reflects the different age distributions of the two samples. As we shall discuss in more detail below, the oldest stars in Shapley III are only ~20 Myr old—corresponding to a main-sequence turnoff near $M_v \sim -3$. On the other hand, star formation in the Galactic disk has occurred over the last 5 Gyr (at least). Thus proportionately more $M_v = -3$ stars have evolved off the main sequence than $M_v = -2$ stars, and the luminosity function steepens as a result. In effect, this means that the Shapley III function is significantly closer to an initial luminosity function at these absolute magnitudes. In addition, Scalo estimates that ~50% of the Galactic stars with $M_v > -4$ are evolved stars, extending to late-type giants, while our color criteria exclude all save blue giants and supergiants. We shall return to the problem associated with assigning spectral types and allowing for stellar evolution when we consider the derivation of a mass function. For $M_v < -3$, however, Scalo's luminosity function is broadly consistent in slope with our data.

There are few other studies of field stars in the LMC against which we can compare our results. Virtually all other surveys are either limited to stars brighter than $V \sim 14$ (as summarized in Dennefeld and Tammann 1980) or comprise deeper photometry within a much smaller area (Butcher 1980; Stryker 1983; Hardy *et al.* 1984). As a result, we can only match our results against the analysis of the Rousseau *et al.* (1978) catalog presented by Freedman (1985). She comments that this catalog is incomplete at a much brighter level than the quoted limits of $V \sim 14$, and restricts the luminosity function derivation to $M_v < -6$. There is thus effectively no overlap with our data, although the slope of 0.6 is consistent with the bright end of our function.

Studies of stars in external galaxies tend to be limited to the most luminous stars, or, rather, the stars with the brightest visual magnitudes. As Massey (1985) has emphasized, since the energy distribution peaks in the ultraviolet for O stars, bolometric corrections for these stars are large and can lead to the most massive O stars having fainter V magnitudes than less massive B stars. Nonetheless, Freedman (1985) has carried out an extensive series of surveys of nearby spiral and irregular galaxies and has shown that in each of the galaxies surveyed, the visual luminosity function is consistent with a power law

$$\phi(M_v) \propto M_v^{0.66} .$$

Unfortunately her data are limited to $M_v < -5$, so there is little overlap with our photometry, but within that range our results are consistent with a power-law slope $0.5 < \gamma < 0.7$, in relatively good agreement with Freedman's results. Finally, Hoessel and Anderson (1986) have derived a luminosity function for NGC 6822 covering the magnitude range $-7 < M_v < -5$, where they find a slope of ~0.59.

b) The Star Formation History

Dopita, Mathewson, and Ford (1985) have proposed that Shapley III is a model example of self-propagating star formation, with an initial central starburst ~15 Myr ago spreading contagiously outward from the center of the H II ring at 5^h31^m, $-66°54'$. They base their conclusions both on the velocity maps of the neutral hydrogen gas, which are consistent with (but do not insistently demand) a 1900 pc diameter shell expanding at 36 km s^{-1}, and on their analysis of the distribution and ages of stars and star clusters within the ring. We have an opportunity to both test this model and probe the star formation history on our own account through the spatial distribution and luminosity function of our stellar sample.

Our photographic plates cover only the southern half of the LMC 4 supergiant shell, although they include the extended OB association LH 77, which Lucke and Hodge identify as Shapley III. DMF argue that the spatial distribution of main-sequence stars strongly supports their model of a uniformly expanding region of star formation, with the youngest stars on the periphery of the H II ring. In particular, they cite Isserstedt's analysis of the distribution of Cepheids and OB stars (Isserstedt 1984), the latter based on Maeder's (1981*a*, *b*) stellar models. However, while it is true that the youngest stars ($\tau < 4$ Myr; Isserstedt's Fig. 19) are exclusively around the H II rim, it is clear that LH 77 makes a significant contribution to all other time slices. Our more comprehensive survey confirms this picture.

Figures 7*a*–7*f* are analogous to Isserstedt's Figures 4–19 in that they compare the spatial distributions of groups of stars of different mean ages. Figure 7*a* shows the location of OB stars ($V-I < 0.2$) with $12 < V < 13$, or $-6.35 < M_v < -5.35$ with our distance modulus for the LMC. Basing our time scale on Maeder's case B models (Maeder 1981*a*, *b*), these correspond to turnoff ages of from 5 to 7.5 Myr. Eight stars with magnitudes in the range $11 < V < 12$ (ages of 3–5 Myr) are also shown. Evolved stars from an older population can also appear in these regions of the H-R diagram, but, as Mermilliod and Maeder (1986) emphasize, such stars have very short lifetimes and are correspondingly rare; hence, the stars plotted are almost certainly main-sequence OB stars.

It is clear that Figure 7*a* shows that, far from being confined to the edge of the H II ring—which intercepts only the souteast and southern edges of our field—these stars show a pronounced concentration within the OB association formed by LH 65, LH 84, NGC 2006, NGC 2034, and, in particular, LH 77. Including stars in the range $-5.35 < M_v < -4.35$ (7.5–11 Myr; Fig. 7*b*) reveals a slightly more extended distribution, with two broad clumps corresponding to the peaks in the UV continuum emission mapped by Page and Carruthers (1978)

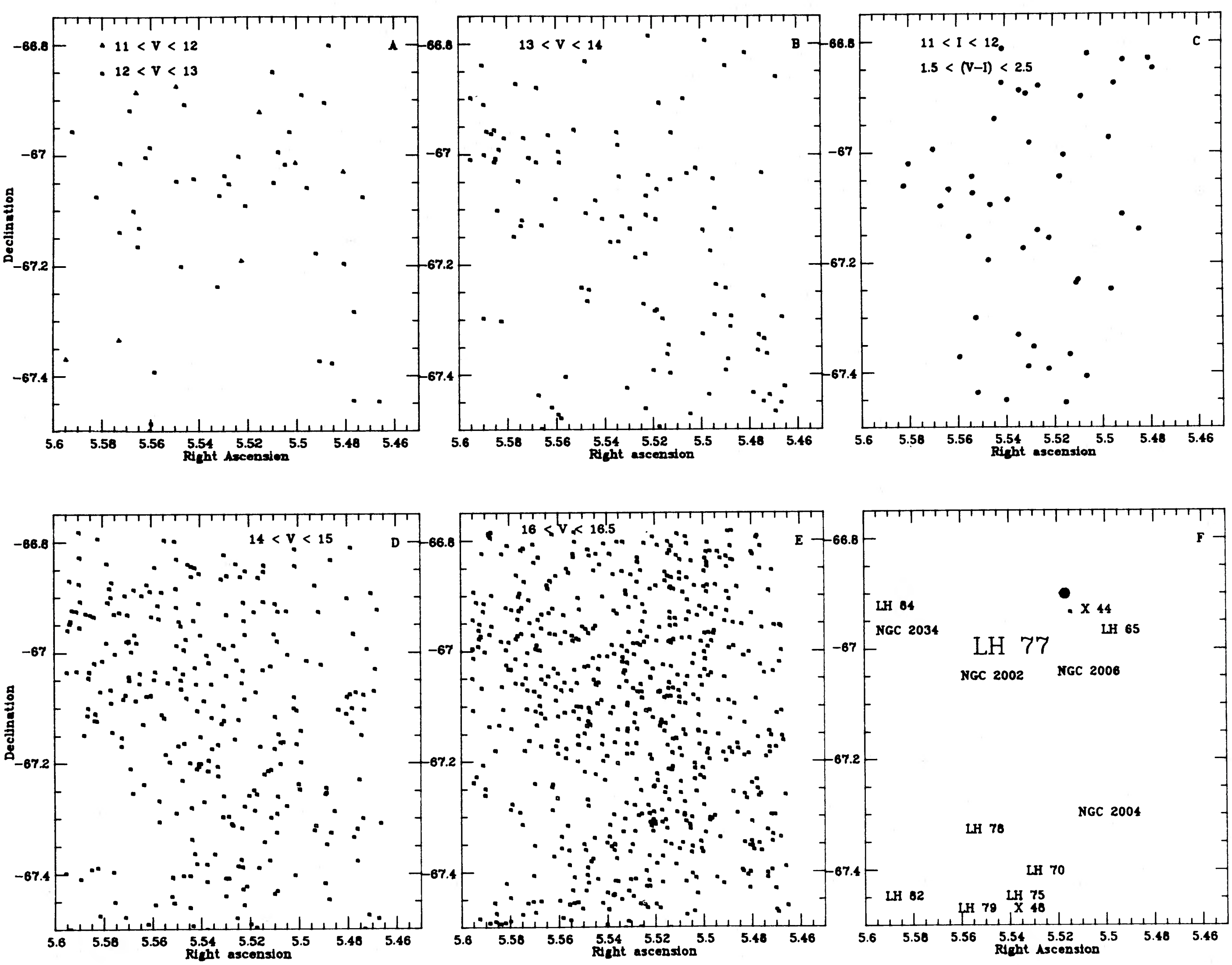

FIG. 7.—Spatial distribution of (primarily) main-sequence stars of differing luminosities: (*a*) $11 < V < 13$; (*b*) $13 < V < 14$; (*c*) the M supergiants at $11 < V < 12$; (*d*) main-sequence stars at $14 < V < 15$; (*e*) $16 < V < 16.5$; and (*f*) the distribution of young clusters and X-ray sources. Solid point in (*f*) marks the center of Shapley Constellation III.

(see Meaburn 1980, Fig. 1). At fainter magnitudes (Figs. 7*c*, 7*d*) the stellar distribution is more uniform. The stars in the red supergiant clump are very similar to that of the OB stars in Figure 7*b*, confirming their status as core helium-burning supergiants (Mould and Reid 1987). Finally, Figure 7*f* shows the positions of the star clusters and associations within our field, as well as the two X-ray sources found in the *Einstein* soft X-ray survey (Long, Helfand, and Grabelsky 1981). Neither of the latter is identified as a possible supernova remnant, although several bona fide remnants populate the rim of LMC 4 beyond our field.

DMF have calculated the projected diameter of the star-forming region at different epochs using Isserstedt's data and the Maeder evolutionary time scales. While their Figure 4 shows a near linear progression in the mean diameter with time, it also shows substantial scatter within each time slice. Examining the OB associations individually presents a somewhat different picture. Figure 8 shows the radial distribution of the Lucke and Hodge (1970) associations in the whole of LMC 4 plotted against age, where the ages are taken from Braunsforth and Feitzinger (1983) and are based on the absolute magnitude of the brightest blue star. Using the statistically averaged time scale, τ_{m_5}, from the latter publication increases the ages by ~0.5 Myr at most, save for the innermost point, LH 65, which then has an age of ~10 Myr. Our data support the younger age shown. These ages of 3–4 Myr within a radius of 400 pc contrast with the estimate of 7–15 Myr for the age of the initial burst of star formation shown in DMF's Figure 4.

Our results are not consistent with a simple model of self-propagating star formation, with a clean progression of stellar ages in concentric annuli. Yet the motivations for considering such a model remain in the presence of the higher velocity H I gas and in the general appearance of the supergiant shell LMC 4. A straightforward modification to the star formation model is to consider star formation continuing for up to 10 Myr within each cloud complex after the initial triggering shock, rather than persisting for only 2–3 Myr, as implied in DMF's Figure 4.

Alternatively, LMC 4 may be the result of two adjacent bursts of star formation, with the bar formed by LH 77 and the associated clusters representing the region where the two initial shocks collided. However, the luminosity function for the LH 77 bar is, save for a slight excess of bright stars, similar in shape to that of the whole field. In particular, the decrement at $M_v \sim -3$ is almost identical in size, suggesting a similar proportion of older stars (Fig. 9*a*). This tends to favor a single trigger, rather than two initial events and a delay before star formation started in this region.

On the other hand, we would expect the youngest stars to dominate in the outermost regions of the Shapley III ring. In such a case the break in the luminosity function should occur at a brighter M_v. Our data only intersect a small section of the rim (in the southwest corner of our field), but we can construct a luminosity function for this region, and this is shown in Figure 9*b*. Although the sampling statistics are poorer, the luminosity function in clearly flatter with a less pronounced break and more luminous stars. This at least qualitatively supports an outward-propagating wave of star formation. In the following section we shall consider the shape of the luminosity function in more detail.

c) The Luminosity Function and Main-Sequence Lifetimes

The stellar luminosity function can, in principle, give substantially more detailed information on the star formation history, provided we can accurately determine masses and hence evolutionary lifetimes. In carrying out this analysis we shall start by restricting ourselves to $M_v > -5$. We do this for two reasons: first, this absolute magnitude corresponds to a spectral type of ~B0. This marks the point where *UBV* colors cease to be degenerate, luminosity class ambiguities start to resolve themselves (Conti, Garmany, and Massey 1986), and we can attempt to interpret our data. Conti, Garmany, and Massey (1986) are carrying out a more detailed star-by-star spectroscopic survey of O stars in the LMC which is better suited to the analysis requirements of such stars. Second, our

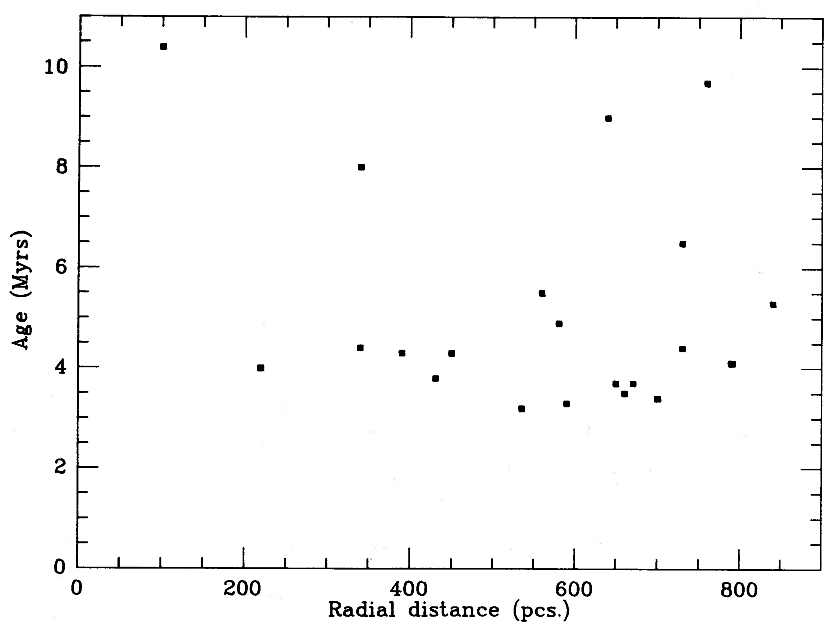

FIG. 8.—Radial distance from the center of Shapley III plotted against age for the Lucke and Hodge associations

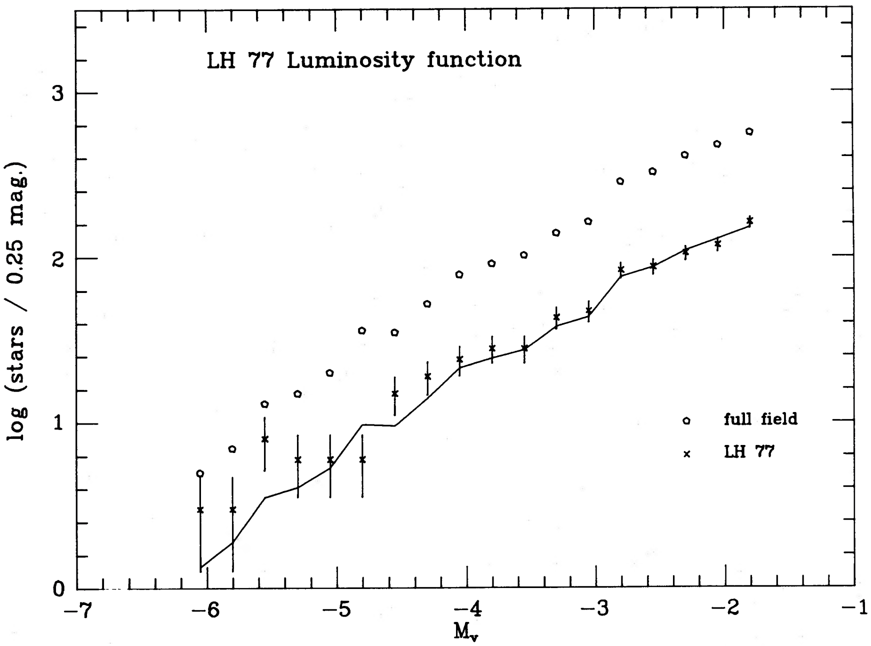

FIG. 9*a*

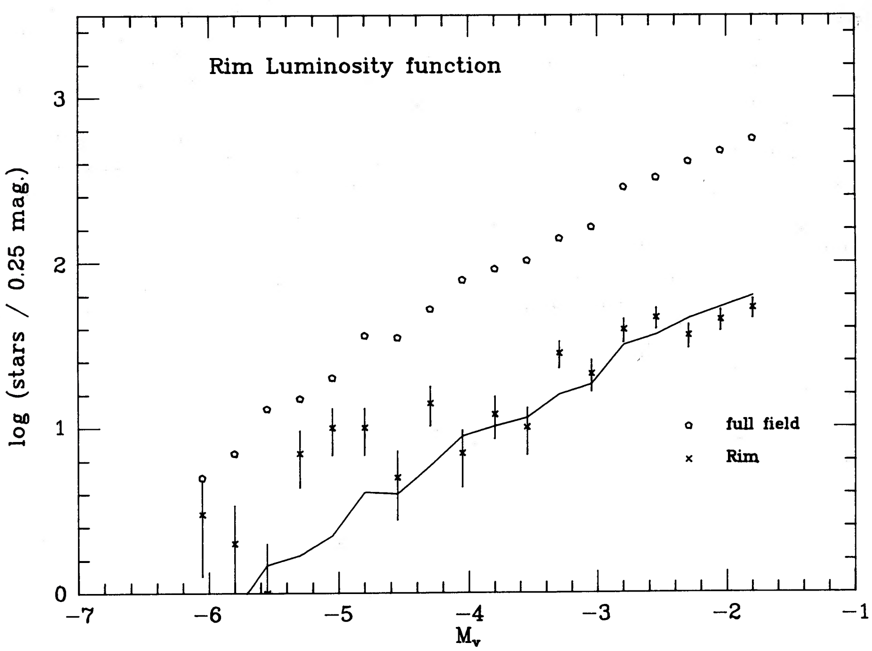

FIG. 9*b*

FIG. 9.—Comparison of the main-sequence luminosity function for (*a*) stars near the central bar (LH 77) and (*b*) stars on the edge of Shapley III. The luminosity function for the whole field is also shown in both cases.

sample includes few stars with $I < 13.5$, and our statistics are correspondingly poor at these bright magnitudes.

Having limited ourselves to these magnitudes, however, we still face problems in transforming the observed quantities to intrinsic parameters. Recent stellar models have emphasized the importance of semiconvection and convective overshoot in extending the lifetimes of intermediate- and high-mass stars (Bressan, Bertelli, and Chiosi 1983). However, there remain disagreements among the different models (and model builders) as to the degree of importance of this effect. Table 5 shows results we have culled from two recent publications: the intermediate-mass models discussed by Bertelli, Bressan, and Chiosi (1985), and the more massive stars modeled by Maeder (1981*a*, *b*) and discussed in Mermilliod and Maeder (1986). We have taken the case B mass-loss models from the latter set and used these to represent the standard set without convective overshoot. The Bressan *et al.* models, on the other hand, are among the most radical convective overshoot calculations.

TABLE 5

COMPARISON OF STELLAR EVOLUTIONARY MODELS

	MAEDER (case B)		BERTELLI *et al.*	
M_v	Mass	τ (Myr)	Mass	τ (Myr)
−5.5..........	30	7	...	...
−5.0..........	25	8	...	...
−4.5..........	20	10	...	...
−4.0..........	15	12	∼9	35
−3.5..........	12	15	...	46
−3.0..........	10	20	∼6	72
−2.5..........	8.5	28	...	107
−2.0..........	7	46	∼4.5	174

These two sets differ by a factor of ∼3–4 in the main sequence lifetimes for given M_v. How, then, are we to discriminate between these contradictory models?

One possibility is raised by DMF's study of the H I kinematics in Shapley III. We have already discussed some of the inconsistencies of their model, but in concluding that these may simply reflect more prolonged star formation within LMC 4, we can still use their dynamical estimate of the age of the complex. Given that the higher velocity H I gas is driven by the expanding shock—and DMF have shown that this presents no problem energetically—and given that the velocity of expansion has remained approximately constant, the observed diameter of ∼1400 pc corresponds to an age of ∼20 Myr. Taking this epoch as the first starburst, we expect a feature in the luminosity function corresponding to stars with this main-sequence lifetime. Fainter than this, the "turnoff" absolute magnitude, all of the stars formed lie on the main sequence, but a proportion of the more luminous stars—those formed at the earlier epochs—will have evolved through the giant branch to dark remnants. We have identified the break near $M_v \sim -3$ as marking the division between these stellar groupings. This favors the Maeder set of models, which predict a lifetime of ∼24 Myr at that absolute magnitude, rather than the lifetime of ∼70 Myr predicted by Bertelli *et al.*

An interpretation of the luminosity function at brighter magnitudes requires modeling the star formation rate. If Shapley III can be regarded as an expanding ring, then, with all other factors being equal, we might expect the overall star formation rate to go with the circumference of the ring, i.e., a linear increase (in the rate) with time. In this view the outward-propagating shock is simply a trigger initiating star formation in an interstellar medium uniformly populated with potential star-forming clouds. However, given the persistence of star formation shown in Figure 7, a better approximation may be a constant star formation rate. We have applied both models in this analysis, since they are likely to bracket the true history: the constant star formation rate (CSF) is likely to overestimate the number of bright stars, while a linear increase of star formation with time (LSF) places most emphasis on the recent past and is likely to underestimate the number density of luminous stars. Given the closer agreement between DMF's results and the Maeder tracks, we have adopted the (M_v, mass, lifetime) relations portrayed in Maeder and Mermilliod and assume that star formation started ∼24 Myr ago.

Figure 10 shows the initial luminosity functions derived from these two models. With a linearly increasing star formation rate the fraction of stars still on the main sequence is higher than for constant star formation. As a result the corrections are smaller and the "turnoff" feature is still prominent. Indeed, if we were to insist on continuity in the luminosity function we probably require a star formation rate decreasing with time, since the break is still evident in the CSF model. It is possible that this is because our field lies predominantly within the LMC 4 H II ring and, as a result, omits the vigorous star formation currently underway at the edge of the region.

To convert to a mass function we have used the mass-luminosity relation given in Table 4, computed from data presented by Popper (1980). The M_v–log M relation is nearly

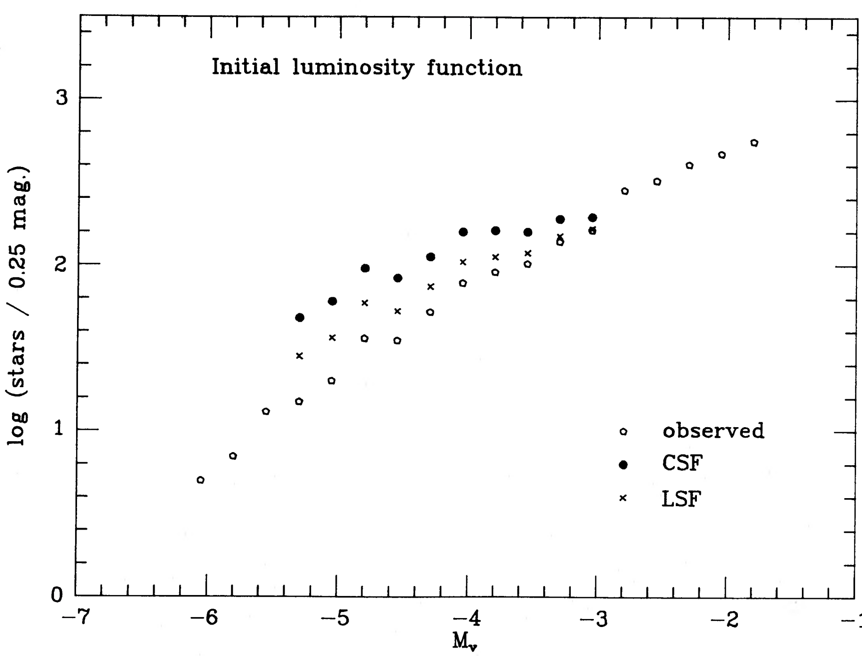

FIG. 10.—The initial luminosity function assuming a constant star formation rate (CSF; *solid points*) or a star formation rate that is linearly increasing with time (LSF; *crosses*). Open circles delineate the observed luminosity function without any evolutionary corrections.

linear at these masses save for a small change in slope at $M_v \sim -3$. This leads to the mass point corresponding to $M_v = -2.8$ lying well above the trend shown by the surrounding points. The resultant mass function is flatter at fainter magnitudes: Figure 11 shows $\Psi(m)$ assuming a constant star formation rate. In terms of a power-law representation in which the Salpeter function has slope 1.35, the slope is ~ 1.5 at $\log M \sim 1.3$, but only ~ 0.6 at $\log M \sim 1$ (ignoring the deviant point at $\log M = 1.1$). Figure 11 also shows the IMF derived by Scalo (1986) from Galactic stars and scaled to fit the LMC number densities. While the slope is very similar to our result at lower masses ($\log M < \sim 1.1$), our data lie systematically above Scalo's at higher masses, possibly suggesting a birthrate that is slightly increasing with time.

Any conclusions one draws about the IMF for these massive stars are dependent upon the assumed star formation history of Shapley III and also upon the unverified assumption that there is a monotonic relation between M_v and mass. Both assumptions are routinely made in developing the local IMF in the Galaxy. A constant rate of star formation is less plausible in the case of a single discrete region, such as Shapley III, than in the spatially averaged Galactic case. For example, one could successfully fit the luminosity function by assuming all the star formation in Shapley III has taken place in the last 20 Myr, that the IMF is the same as Scalo's (1986) Galactic IMF, and that the star formation rate has been rising quite recently. Discriminating among the various options requires data as detailed as those presented here, but covering the full area of Shapley III, allowing a more exact determination of the radial variation of the luminosity function.

IV. THE EXTENDED GIANT BRANCH

The second prominent feature in Figure 5 is the giant branch due to the underlying intermediate-age population of the LMC. Figure 12 shows the (I, $V-I$) color-magnitude diagram for a 0.6 deg^2 region centered on R.A. = 5^h18^m, decl. = $-66°30'$: a region lacking any evidence for recent star formation activity. These data are from the Schmidt plates discussed in Paper I. Although not extending to such faint magnitudes, the morphology of the giant branch is very similar to that in Shapley III.

We have already shown that Galactic stars make a negligible contribution to the main-sequence star counts. Such is not quite the case for the redder giant stars. Although LMC stars dominate the counts in the center of the giant branch, Galactic stars can blur the distribution at the edges and apparently broaden the feature. To allow for this we have used the model listed in Table 3 to generate synthetic star counts. Figure 13 shows the resulting color-magnitude diagram. These data are then subtracted from the real star counts by pairing the synthetic stars with objects within ± 0.15 in magnitude and color. Figure 14*a* shows the resultant "clean" color-magnitude diagram for an assumed completeness of 60% (scaling the counts in Table 3). This entails removing 706 of the 10,704 stars plotted in Figure 5. A further 202 field stars were generated but failed to find real pairs. Most of these have $I > 16$ and lie to the red of the LMC giant branch, and incompleteness in the V star counts at faint magnitudes probably accounts for their absence. The remainder have $V-I < 0.6$ and are halo stars, and this suggest that the M92 giant branch adopted for the halo may be too metal poor. The results, however, are adequate for our purposes.

While most of the stars removed by this cleaning lie between the young main sequence and the giant branch, it is evident that some stars remain. This is the case even if we assume a completeness of 85% in our star counts (Fig. 14*b*). Both figures reveal the clear presence of an extended giant branch, lying to the blue of the dominant giant branch stars, with $V-I$ colors between 1 and 2, and terminating in the clump of red supergiants at $I \sim 12$. We identify these stars as the young, massive, hydrogen core-burning stars associated with star formation in Shapley III whose spectra we discuss separately elsewhere (Mould and Reid 1987.). Those stars remaining, with $V-I < 1$

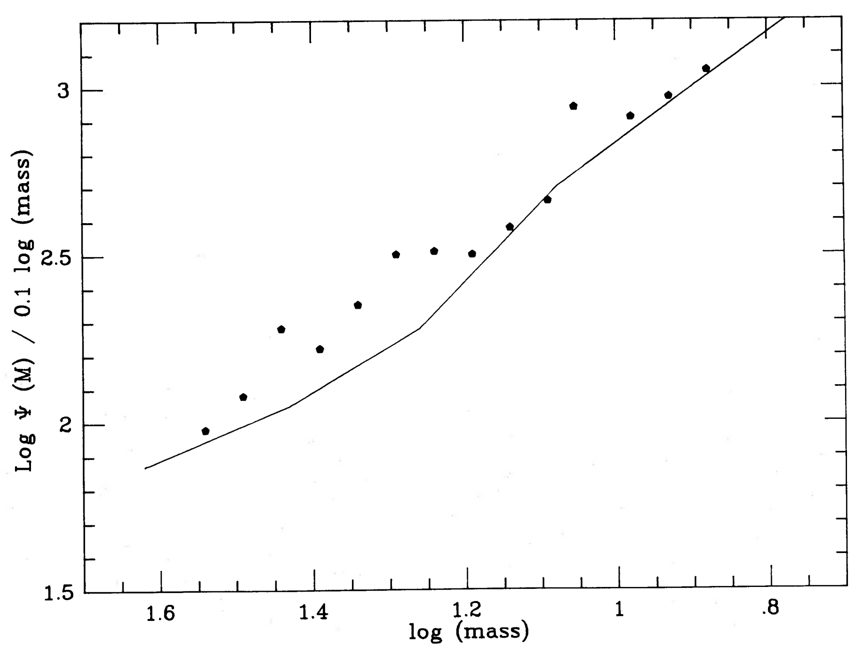

FIG. 11.—The mass function derived assuming a constant star formation rate

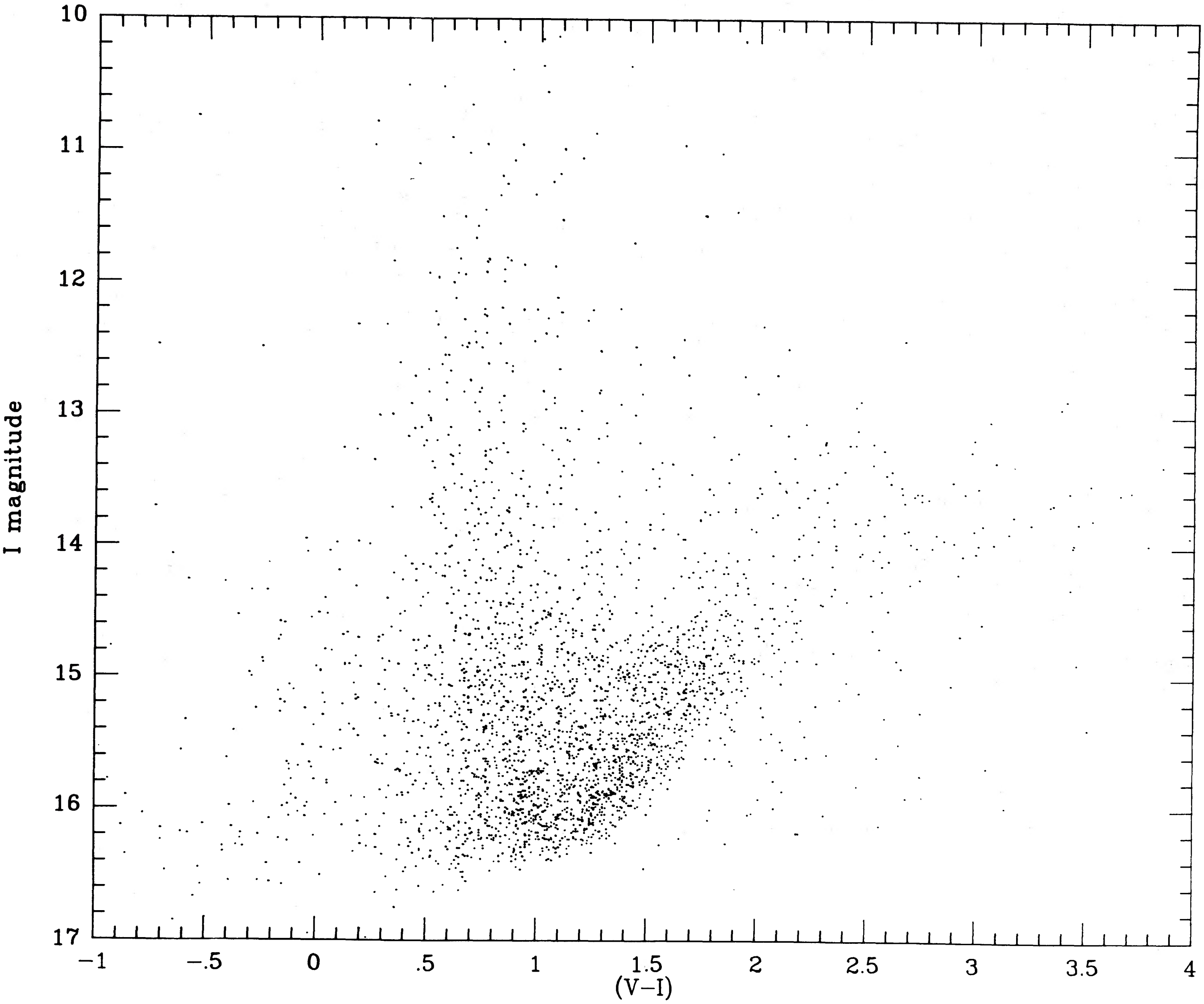

FIG. 12.—I, $V-I$ color-magnitude diagram for a region of the LMC lacking recent star formation

and $I < 16$, are likely to be the yellow supergiants and Cepheids from the same population.

We can use these cleaned color-magnitude diagrams to study both the luminosity function and the width in $V-I$ of the giant branch from the underlying older stellar population. In these calculations we have used the data plotted in Figure 14*b* as minimizing the field star contribution. Following Mould, Kristian, and Da Costa (1983), we have applied a cut across the giant branch at $M_I = -3.0 \pm 0.25$ (corresponding to $\langle I \rangle = 15.17$–$15.67$ for $A_I = 0.07$) to study the color distribution. As Figure 15 shows the peak lies at $V-I \sim 1.48$ ($[V-I]_0 = 1.43$), nearly midway between the M92 and 47 Tuc giant branches. Using Mould *et al.*'s calibration of $V-I$ against [M/H], this implies a mean metallicity of $[M/H] \sim -1.1 \pm 0.2$, similar to that in NGC 147. This is slightly more metal rich than the estimate of $[M/H] \sim -1.4$ obtained by Butler, Demarque, and Smith (1983) from spectroscopy of RR Lyraes stars near the bar of the LMC. However, since our observations cover younger stars, it is not surprising that these stars should be more metal rich.

The color distribution of LMC giants at $M_I = -3$ has a broader base than one would expect from the error estimates given in § II. It is clear that the distribution in Figure 15 is skewed toward bluer $V-I$. However, this may reflect the inclusion of hotter, first red giant branch stars rather than a significant spread in the metallicity.

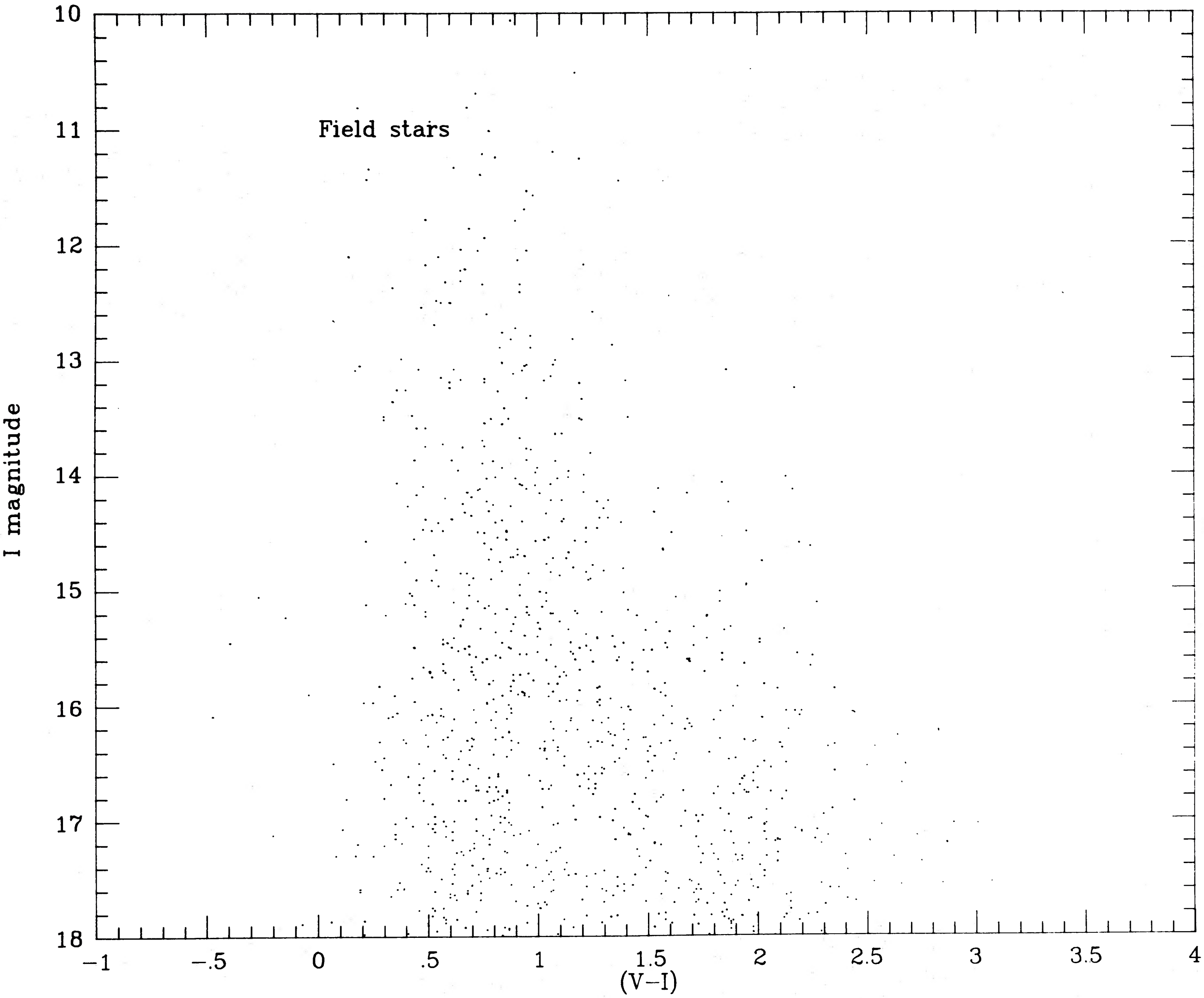

FIG. 13.—Color-magnitude diagram for field stars predicted by the galactic model described in the text

In calculating the giant branch luminosity function we have included all stars redder than $V-I = 1.5$ with magnitudes brighter than $I = 15$. At fainter magnitudes the blue cutoff varies linearly to $V-I = 0.6$ at $I = 17$. Figure 16 shows the luminosity function summed in bins of 0.1 mag width. Mould and Kristian (1986) have suggested that the magnitude at the tip of the giant branch can be used as a distance indicator, using the absolute magnitude calibration presented by Frogel, Cohen, and Persson (1983). Defining the position of the giant branch tip for the LMC is complicated by the presence of a substantial population of intermediate-age AGB stars and, in Shapley III, CHB supergiants, both of which contribute stars at higher luminosities. However, Figure 16 shows that there is a discontinuity in the number counts at $\langle I \rangle = 14.60 \pm 0.05$, with the number of stars increasing by a factor of 2. From Figure 14*b*, the mean color at this magnitude is $V-I = \sim 1.8$, which corresponds to a bolometric correction (BC_I) of 0.39 (for M stars; Bessell and Wood 1985). Frogel *et al.*'s equation (4) implies an absolute bolometric magnitude of $\sim -3.5 \pm 0.1$, and, allowing for absorption of $A_I = 0.07$, this gives a distance modulus of 18.42 ± 0.15. This is consistent with the value favored by Reid and Strugnell (1986) and lies nearly midway between the extremes of the long (Feast 1984) and short (Schommer, Olszewski, and Aaronson 1984) distance scales. It

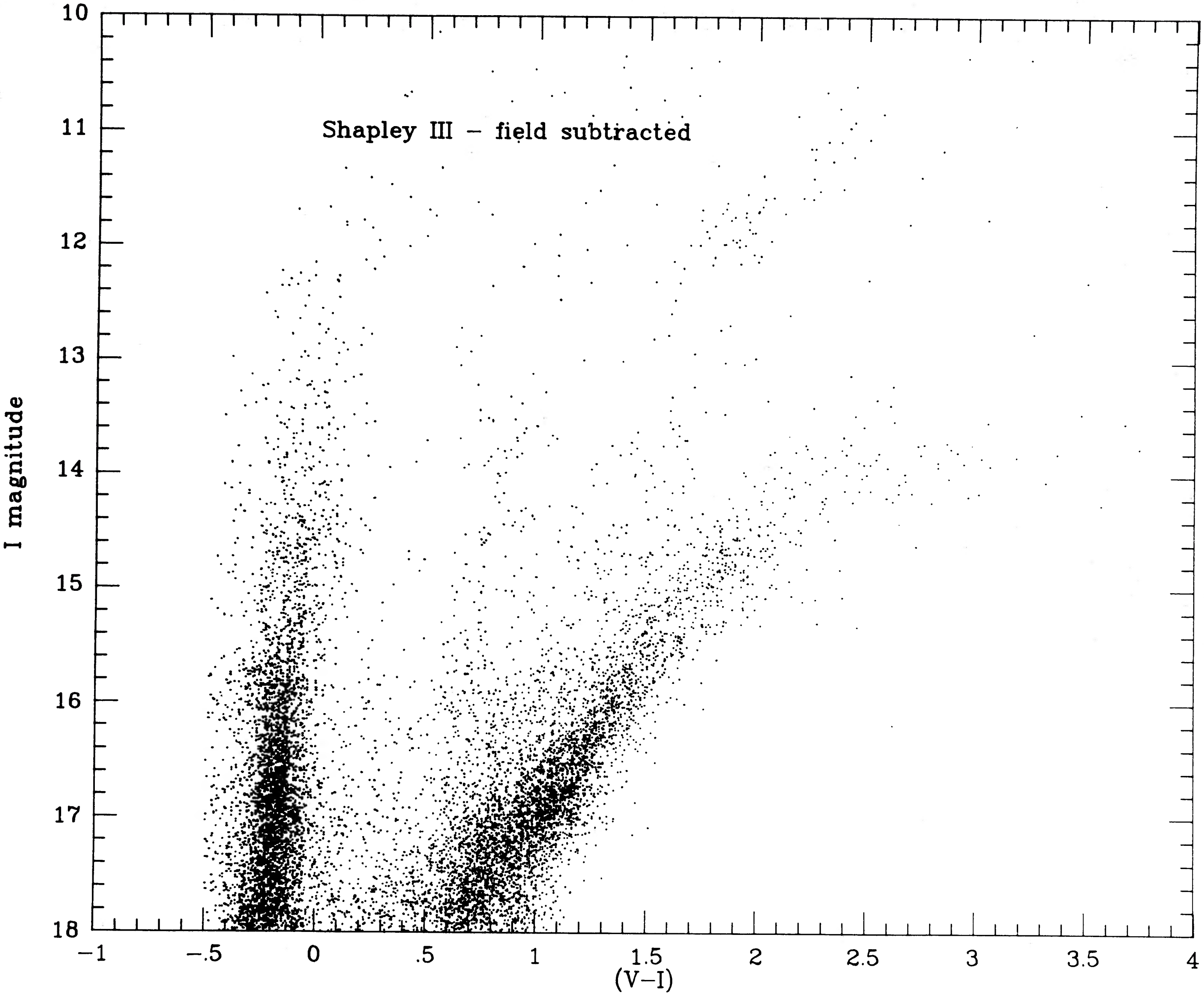

FIG. 14*a*

FIG. 14.—Color-magnitude diagrams for Shapley III after field stars subtraction (*a*) assuming 60% completeness and (*b*) assuming 85% completeness

is remarkable that this method works even in the presence of a subtantial intermediate-age (and young) stellar population.

V. CONCLUSIONS

We have used photographic photometry of Las Campanas V and I band plates to construct a color-magnitude diagram for part of Shapley's Constellation III in the LMC. Our data show a large population of young stars, evidenced by a blue main sequence and a clump of red supergiants, as well as the CHB and AGB giant stars of the underlying intermediate-age population. The main-sequence luminosity function for the young population exhibits a break at $M_v = -3$, which we interpret as the turnoff of the initial burst of star formation. Dopita *et al.* have estimated a dynamical age for Shapley III of $\sim$20 Myr, close to the age of $\sim$24 Myr derived using the position of the turnoff and Maeder's (1981*a*, *b*) models. In contrast, models with convective overshoot predict an age of $\sim$70 Myr. We have made some attempt to derive an initial mass function and find that a constant star formation rate requires a rather flat IMF. However, this conclusion is very sensitive to the exact star formation rate adopted.

Subtracting the foreground Galactic stars leaves a well-defined intermediate-age giant branch, with a mean color of $(V-I)_0 = 1.43$. This corresponds to a mean metallicity of $[M/H] \sim -1.1$. Finally, star counts suggest that the tip of the red giant branch has an apparent magnitude of $\langle I \rangle = 14.60$, giving a distance modulus of 18.42 ± 0.15 for the LMC.

This research was partially supported by NATO grant RG. 85/0495 and NSF grant 85-02518.

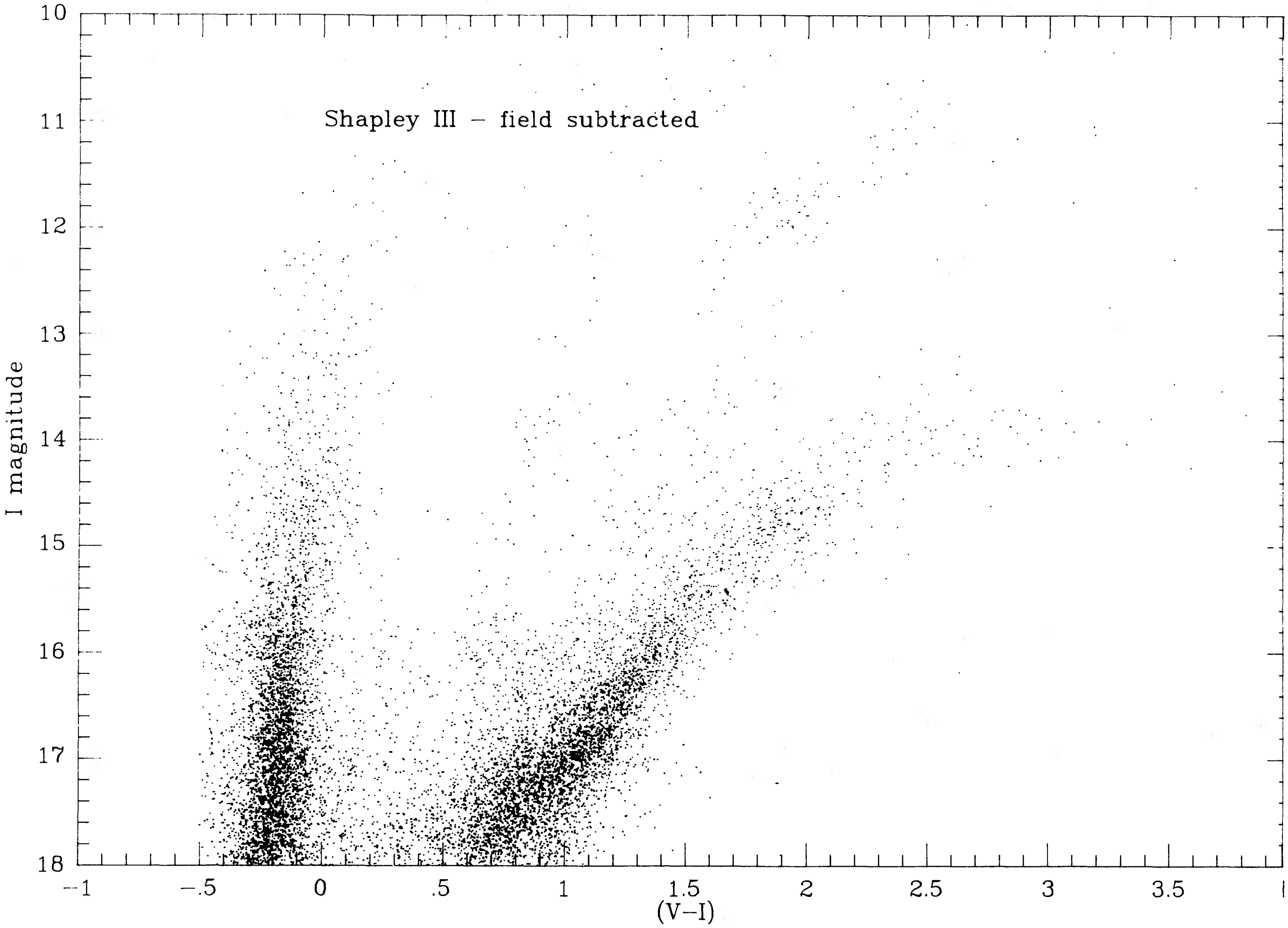

FIG. 14*b*

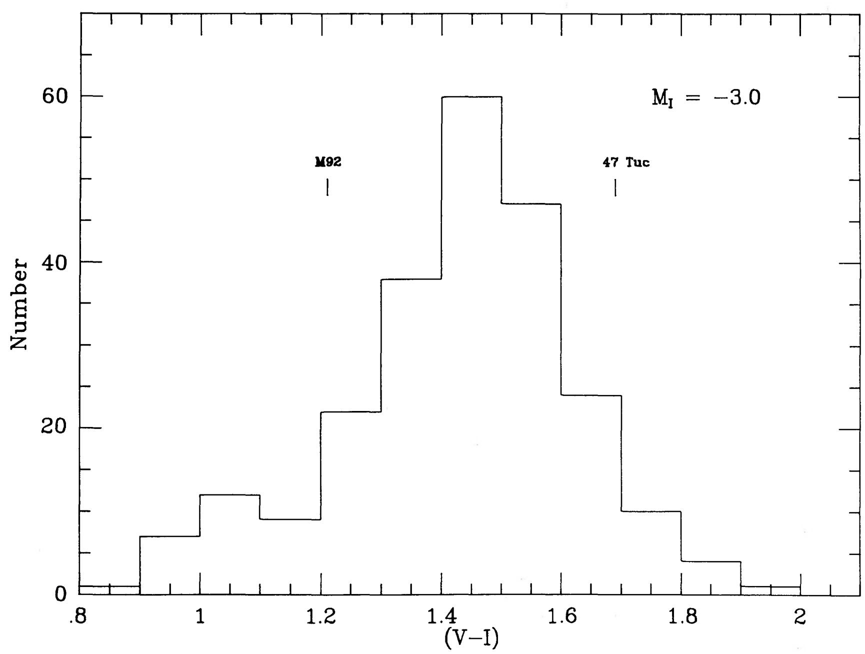

FIG. 15.—Color distribution across the LMC giant branch at $M_I \sim -3$

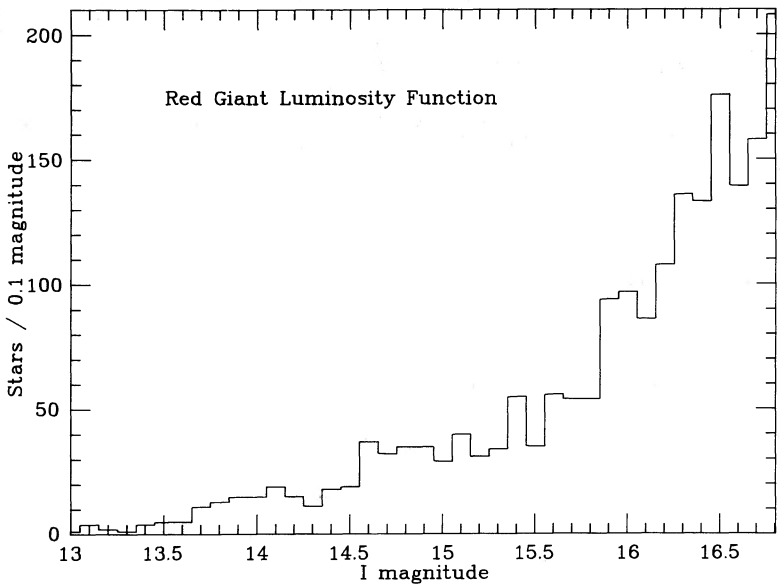

FIG. 16.—LMC red giant luminosity function in the Shapley III area

REFERENCES

Bertelli, G., Bressan, A., and Chiosi, C. 1985, *Astr. Ap.*, **150**, 33.
Bessell, M. S., and Wood, P. R. 1985, *Pub. A.S.P.*, **96**, 247.
Braunsforth, E., and Feitzinger, J. V. 1983, *Astr. Ap.*, **127**, 113.
Bressan, A. G., Bertelli, G., and Chiosi, C. 1983, *Astr. Ap.*, **102**, 25.
Butcher, H. 1980, *Ap. J.*, **216**, 372.
Butler, D., Demarque, P., and Smith, H. A. 1983, *Ap. J.*, **157**, 592.
Conti, P., Garmany, C. D., and Massey, P. 1986, *Ap. J.*, **297**, 599.
Dennefeld, M., and Tammann, G. A. 1980, *Astr. Ap.*, **83**, 275.
Dopita, M., Mathewson, D., and Ford, V. 1985, *Ap. J.*, **297**, 599.
Feast, M. W. 1984, *M.N.R.A.S.*, **211**, 51P.
Freedman, W. L. 1985, *Ap. J.*, **299**, 74.
Frogel, J., Cohen, J. G., and Persson, S. E. 1983, *Ap. J.*, **275**, 773.
Gallagher, J. S., Hunter, D. A., and Tutukov, A. V. 1984, *Ap. J.*, **284**, 544.
Gilmore, G. F. 1984, *M.N.R.A.S.*, **207**, 223.
Goudis, C., and Meaburn, J. 1978, *Astr. Ap.*, **68**, 179.
Hardy, E., Buononno, C. E. C., Janes, K. A., and Schommer, R. A. 1984, *Ap. J.*, **275**, 773.
Hoessel, J. G., and Anderson, N. 1986, *Ap. J. Suppl.*, **60**, 507.
Isserstedt, J. 1984, *Astr. Ap.*, **131**, 347.
Long, K. S., Helfand, D. J., and Grabelsky, D. A. 1981, *Ap. J.*, **248**, 925.
Lucke, P. R., and Hodge, P. W. 1970, *A.J.*, **75**, 171.
Maeder, A. 1981*a*, *Astr. Ap.*, **99**, 97.
———. 1981*b*, *Astr. Ap.*, **102**, 401.
Massey, P. 1985, *Pub. A.S.P.*, **97**, 5.
McCuskey, S. W. 1966, *Vistas Astr.*, **7**, 141.
McGee, R. X., and Milton, J. A. 1966*a*, *Australian J. Phys.*, **19**, 343.
———. 1966*b*, *Australian J. Phys. Ap. Suppl.*, **2**, 1.
McNamara, D. H., and Feltz, K. A., Jr. 1980, *Pub. A.S.P.*, **92**, 587.
Meaburn, J. 1980, *M.N.R.A.S.*, **192**, 365.
Mermilliod, J.-C., and Maeder, A. 1986, *Astr. Ap.*, **158**, 45.
Miller, G. E., and Scalo, J. S. 1979, *Ap. J. Suppl.*, **41**, 513.
Mould, J. R., and Kristian, J. 1986, *Ap. J.*, **305**, 91.
Mould, J. R., Kristian, J., and Da Costa, G. S. 1983, *Ap. J.*, **270**, 471.
Mould, J. R., and Reid, I. N. 1987, *Ap. J.*, in press.
Nail, V. McK., and Shapley, H. 1953, *Proc. Nat. Acad. Sci.*, **39**, 358.
Page, T., and Carruthers, G. R. 1978, NRL Rept. No. 8206.
Popper, D. M. 1980, *Ann. Rev. Astr. Ap.*, **18**, 115.
Reid. I. N., and Mould, J. R. 1984, *Ap. J.*, **284**, 98.
Reid, I. N., and Strugnell, P. R. 1986, *M.N.R.A.S.*, **221**, 887.
Rousseau, J., Martin, N., Prevot, L., Reibeirot, E., Robin, A., and Brunet, J. P. 1978, *Astr. Ap. Suppl.*, **31**, 243.
Scalo, J. S. 1986, *Fund. Cosmic Phys.*, **11**, 1.
Schommer, D. A., Olszewski, E., and Aaronson, M. 1984, *Ap. J.* (*Letters*), **285**, L53.
Stryker, L. L. 1983, *Ap. J.*, **266**, 82.

J. R. MOULD and I. N. REID: Caltech 105-24, Pasadena CA 91125

I. THOMPSON: 813 Santa Barbara Street, Pasadena, CA 91101